Inorganic Chemistry Communications 183 (2026) 115669

Contents lists available at ScienceDirect

Inorganic Chemistry Communications

journal homepage: www.elsevier.com/locate/inoche

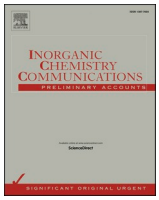

Research Article

Impact of post-deposition curing of graphite thick-film working electrode on the performances of electrochemical sensors

Danjela Kuscer [a,b,*,1], Barbara Repič [a,b,1], Janez Kovač [a,b], Nejc Suban [a,b], Hana Uršič [a,b]

[a] Jožef Stefan Institute, Electronic Ceramics Department, Jamova cesta 39, Ljubljana, Slovenia
[b] Jožef Stefan International Postgraduate School, Jamova cesta 39, Ljubljana, Slovenia

ARTICLE INFO

Keywords:
Screen printing
Electrochemical sensor
Graphite thick films
Post-deposition curing
Cyclic voltammetry
Surface morphology

ABSTRACT

Miniature electrochemical sensors (ES) with screen-printed electrodes and electrical contacts offer qualitative and quantitative detection of various redox-active compounds in water rapidly, with good sensitivity and selectivity. To avoid short circuits, herein we covered the electrical contacts with UV- and temperature-curable polymers to isolate them from the solution. We investigated the influence of UV-light exposure and thermal treatment at 150 °C in air on the surface morphology, chemical composition and electrical conductivity of graphite-based working electrode (WE), as well as on overall electrochemical performance of the ES. Untreated (AP), UV-, and temperature-cured WE possess comparable surface roughness and sheet resistance, 3 μm and 9 Ω/sq., respectively. Cyclic voltammetry (CV) reveals good reversibility for all electrodes, with AP and UV-cured WEs having comparable peak separation (≈115 mV), current response, electrochemically active surface area A_{ecsa} (0.64 cm^2), and electron transfer rate constant k^0 (8.0 × 10^{-3} cm s^{-1}). Heating to 150 °C in air increased peak separation to 170 mV, reduced A_{ecsa} and k^0 to about 27 % and 22 %, attributed to oxygen incorporation in WE, confirmed by X-ray photoelectron spectroscopy. The analysis of ESs in aqueous solution of insecticide imidacloprid confirmed similar responses of AP and UV-cured ESs, whereas response of temperature-cured ES was significantly lower. The temperature-cured ESs demonstrated improved electrochemical responses after linear sweep voltammetry in a potential range down to −1.5 V, which is likely due to the removal of oxygen from WE. Our results demonstrate that post-deposition curing significantly influences the performance of electrochemical sensors for water pollution monitoring.

1. Introduction

Sensors based on electroanalytical methods offer qualitative and quantitative detection of various redox-active compounds with good sensitivity and selectivity with little or no sample preparation. They enable rapid analysis, are inexpensive, consume minimal energy, allow a high degree of automation and can be easily operated by non-trained personnel. The conventional electrochemical analysis is performed within an electrochemical cell with counter (CE), reference (RE) and working electrodes (WE) submerged within a solution of interest, and the electrochemical response is measured using commercial potentiostat [1]. This setup with bulky electrodes and instrument is suitable for measurements in laboratories, while outside the laboratory conditions, the analytical tools are required to be economical, miniature and robust. The electrochemical sensors which consist of all electrodes and electrical interconnections integrated onto selected substrate, commonly called screen-printed electrodes (SPE), consistently deliver reliable analysis results with similar sensitivity and selectivity as conventional devices. The SPEs, with a size of electrodes of a few millimetres and their thickness, typically between 10 and 40 μm, are significantly smaller compared to conventional device, and require much lower volume of the analyte for measurements, a few mL. The mature thick film technology allows economical production of SPEs in a large scale, in a reproducible manner, as well as flexible design and versatility in terms of materials. The SPEs are frequently used as disposable devices and are suitable for on-site analysis [2–4]. Thus, they find applications in various fields, such as food safety, environmental monitoring, biosensing, medical diagnostics and forensics [5,6].

* Corresponding author at: Jožef Stefan Institute, Electronic Ceramics Department, Jamova cesta 39, Ljubljana, Slovenia.
E-mail address: danjela.kuscer@ijs.si (D. Kuscer).
[1] These two authors contributed equally to this work

https://doi.org/10.1016/j.inoche.2025.115669
Received 5 August 2025; Received in revised form 28 September 2025; Accepted 12 October 2025
Available online 14 October 2025

The SPEs are processed by successive deposition of CE, RE, WE and electrical contacts. Each layer has to be cured and the curing procedure depends on the type of paste either using ultra-violet (UV) light treatment or heated at elevated temperatures of a few hundred °C. In case of carbon-based WE, the deposited layer is either cured at low temperatures in air [7–10] or annealed at 850 °C in argon atmosphere [11]. UV curing and curing at low temperature results in a carbon-binder composite WE, while heating at 850 °C results in WE of a pure carbon, without any organic-paste residues [12,13]. For precise and accurate analysis, the entire surface of all the electrodes is in contact with analyte, commonly aqueous solution, while the electrical contacts have to be isolated from the solution to avoid short circuits. One of the possibilities to prevent the electrical contacts from the solution, is to cover them with a layer of fluid-tight polymer [14]. To keep the production process as simple and as economic as possible, without complex and time-consuming procedures, the polymer should be deposited over the electrical contacts by screen printing in the very last stage of the SPE production. Such polymers are commercially available, but require post-deposition treatment. The most common approach includes treating the polymer layer at a few hundred °C or using UV light treatment. However, the influence of post-deposition treatment of SPE, namely heating and UV curing, on the properties of carbon-based WE and on the electrochemical response of the SPE, is unclear.

Here, we report on the SPE composed of platinum CE, RE and electrical contacts, and WE, made from graphite-based in-house paste. We conducted a systematic study on the thickness and surface of as-prepared, UV-cured and temperature-cured WE and related them to their electrochemical properties, measured in a model solution of a known redox system $Fe(CN)_6^{3-/4-}$ (HCF) and in a model solution of imidacloprid (IMD). IMD is a systemic insecticide known to pose toxic risks to non-target organisms such as insects, birds, fish, and mammals. It has been detected in soil, water, and food samples, representing a potential hazard to human health as well [15]. We demonstrate that by a simple electrochemical pre-treatment procedure the electrochemical response of SPE is improved. Such a study is relevant to understand and to improve the quality of carbon-based SPEs i) for researchers, to understand the processing of SPE and to improve reproducibility with simple pre-treatment procedure, and for ii) vendors, to effectively protect electrical contact, while keeping the electrochemical response of SPE at high level and without increasing production time and cost.

2. Experimental

Electrochemical sensors (ES) with platinum CE, RE and electrical contacts were prepared from a commercial platinum paste (9141 R, Du Pont), which was deposited by screen printer (P-250AVF, KEKO Equipment, Slovenia) onto alumina substrate (96 % Al_2O_3, Rubalit 708S, CeramTec). Printed layers were fired at 1000 °C for 1 h in air. Graphite and graphite/glass (weigh ratio of 75/25) spherical working electrodes (WE) with a diameter of 4 mm were prepared from paste made from graphite powder with a median particle size (d_{v50}) of 15 μm (graphite flake, 99.8 %, Alfa Aesar, Karlsruhe, Germany), glass with d_{v50} of 2.4 μm (Steklarna Hrastnik, Slovenia,) and organic vehicle as described elsewhere [11,16]. After screen-printing, the layers were fired at 850 °C for 30 min in argon. The electrical contacts of as-prepared samples were covered with 1) temperature-curable polymer (240-SB, Ferro) and annealed at 150 °C for 2 h in air, or 2) with an UV-curable polymer (5018, Du Pont) and cured with a 400 W ozone-free, iron-doped metal halide lamp for 10 min. For characterization of as-prepared samples, the contacts were manually covered with a nitrocellulose-based polymer and dried at room temperature. The processing of ES is schematically shown in Fig. 1.

The thickness t and root-mean-square surface roughness R_q of the films were measured using a contact stylus profilometer (DektakXT Advanced System, Bruker, USA) with the software Vision 64 (Bruker, USA) as previously reported [12].

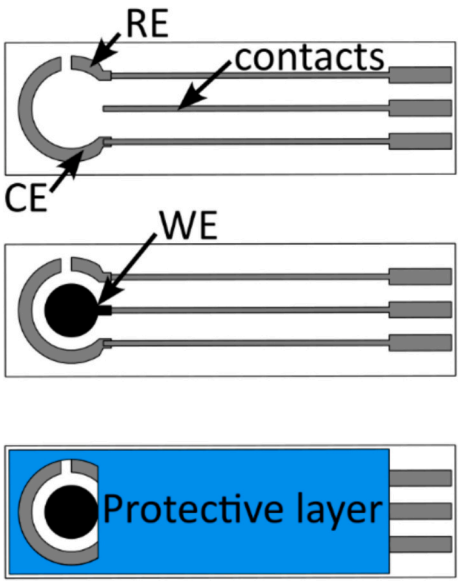

Fig. 1. Scheme of ES fabrication and electrode configuration.

Adhesion of thick films on alumina was evaluated by applying an adhesive tape onto the layer and then the tape was pulled down at an angle as close to 180 degrees as possible. The thickness of the layer before and after the tape test was measured by contact stylus profilometer.

The surface of the films was investigated using a scanning electron microscope (SEM, Quanta 650 ESEM, Thermo Fisher Scientific, USA) and atomic force microscope (AFM, MFP-3D, Asylum Research, Oxford Instruments, USA). The areas of 80 μm × 80 μm and 20 μm × 20 μm were scanned in AC topography mode with a silicon AFM tip (OMCL-AC160TS-R3, Olympus, Japan). The root-mean-square surface roughness R_q^{AFM} was calculated from the obtained AFM map scans [12].

The X-ray photoelectron spectroscopy (XPS) analyses were carried out on GENESIS spectrometer (Ulvac PHI, Japan) equipped with an Al-monochromatic source. The surface composition was quantified from the XPS peaks C 1s and O 1s, considering the relative sensitivity factors provided by the instrument manufacturer [17].

The sheet resistance R_s of the WE was determined on 8 mm × 8 mm square graphite-glass films, annealed and treated at identical conditions as ESs, by a four-point probe technique using a high-voltage source-measure unit (Keithley 237, USA) and a geometric correction factor of 0.795 [12].

The electrochemical behaviour of the ESs was carried out using a potentiostat/galvanostat (Multi Autolab M 204, Methrom, The Netherlands) operated with Nova 2.1.5 software. Cyclic voltammograms (CV) were performed at 25 ± 0.5 °C in a 5 mL electrochemical cell in a 0.1 M phosphate buffer solution (PBS) with pH = 7, in model solution containing 5 mM $Fe(CN)_6^{3-/4-}$ (HCF) in 0.1 M PBS and in model solution containing 100 μM imidacloprid (IMD) in 0.1 M PBS. The preparation of buffer solution (PBS) from NaH_2PO_4 (99.0 %) and Na_2HPO_4 (>99.0 %), both from Merck, Germany, HCF from $K_4[Fe(CN)_6]\bullet 3H_2O$ (≥98.5 %) and $K_3[Fe(CN)_6]$ (99 %), both from Carlo Erba, France, and IMD from $C_9H_{10}ClN_5O_2$ (≥98.0 %) from Sigma Aldrich, USA was described in [12]. The pH of the solutions was adjusted using 1 M HCl or 1 M NaOH solution and measured with a pH meter (Mettler Toledo, USA). Before CV measurements the solution was purged with nitrogen for 5 min.

The CVs in HCF and PBS on the selected ESs were recorded between −0.35 V and +0.35 V from the initial potential of −0.2 V in the positive direction with a step potential of 2.44 mV at scan rates of 50, 75, 100, 150, 200, and 500 mV s^{-1}. The first set of measurements were performed in PBS by conducting 5 cycles at 100 mV s^{-1} to determine the capacitive current I_{cap}. The second set of measurements in PBS was performed by

recording 3 cycles at six selected scan rates. This was followed by the measurements in HCF under the same conditions as in PBS. From these measurements, we determined the peak potential E_p and the peak current I_p, which were used to calculate the ratio of cathodic to anodic peak current I_{pc}/I_{pa} and the peak-to-peak potential separation ΔE_p [12]. The reported values are average values of the parameters determined for 3 parallel samples. From the CVs recorded in HCF at different scan rates, the electrochemically active surface area (A_{ecsa}) was calculated using modified Randles-Ševčík equation for quasi-reversible reaction [12,18,19] and the standard heterogeneous electron transfer rate constant (k^0) was determined using the Nicholson method [12,20]. To calculate the actual surface area, A_{real} expressed in cm^2/cm^2_{geo} the A_{ecsa} was normalized with the geometric surface area of the electrode.

The potential window (PW) of the ESs was determined based on a qualitative inspection of a series of CVs measured at scan rate of 100 mV s^{-1} in non-faradaic region in HCF by first incrementally decreasing the lower vertex potential of the sweep range by 50 mV increments from −0.35 V to −1.5 V between subsequent scans and then increasing the upper vertex potential by 50 mV increments from +0.35 V to +1.0 V. The PW of carbon based ES is limited by the hydrogen evolution reaction (HER) in negative [21] and the carbon oxidation in positive potential range [22]. The limits of the PW were identified as the onset potentials of HER and carbon oxidation at which the current was in the same range as the peak current of the HCF redox probe.

Conditioning during cathodic scan was investigated by performing 5 consecutive CV cycles in PBS at 100 mV s^{-1} between −1.5 V and +0.35 V from initial potential −0.2 V in the positive direction, while ES pretreatment included performing a single linear scan voltammogram from 0.0 V to −1.5 V in HCF solution.

The CVs in IMD and PBS on the AP, UV- and temperature-cured ESs were recorded between −1.5 V and +0.35 V from the initial potential of −0.2 V in the positive direction with a step potential of 2.44 mV at scan rate of 100 mV s^{-1}. First cycle was performed in IMD after 1 min of accumulation at −0.2 V under stirring conditions at 750 min^{-1}. Then five consecutive cycles were performed in PBS to remove any adsorbed species and the last cycle was used as background current for determination of peak currents as described elsewhere [12].

3. Results and discussion

All the components of ES screen-printed onto alumina, namely RE, CE and electrical connections made from platinum, and graphite-based WE, have the required shape corresponding to the intended design geometry. After firing, the platinum showed excellent adhesion to the alumina substrate while the graphite remained adhered to the alumina during the electrochemical tests, but there was a risk of delamination under mechanical stress. Evidence from tape tests indicated that part of the graphite layer delaminated from the substrate. The incorporation of glass into the graphite paste significantly improved adhesion, as shown in Fig. 2. When heated to 850 °C, the glass in the graphite-glass composite melts and thus improves the bonding of the graphite with the alumina substrate.

The as-prepared graphite-glass WEs (WAP) were about 35 μm thick with a surface roughness R_q of 3.1 μm, measured by surface profilometry, and electrical sheet resistance R_s of 9.2 Ω/sq. This value resembles the R_s of graphite thick film [11,12], suggesting that the addition of 25 wt% glass to graphite has a minimal impact on the film's R_s. After treating the WAP with UV (WUVC), or heating to 150 °C in air (WTC), the layers had similar thickness, roughness and sheet resistance as WAP (Table 1).

The scanning electron microscopy (SEM) images of the WAP, WUVC, and WTC (Fig. 3a, b, and c, respectively) demonstrate that the surfaces of all samples are similar, with homogeneously distributed phases. The grey areas represent graphite (GR), exhibiting grain sizes ranging from a few micrometres to several tens of micrometres. The bright grains, measuring up to ten micrometres, correspond to the glass (GL). Dark areas are pores (P).

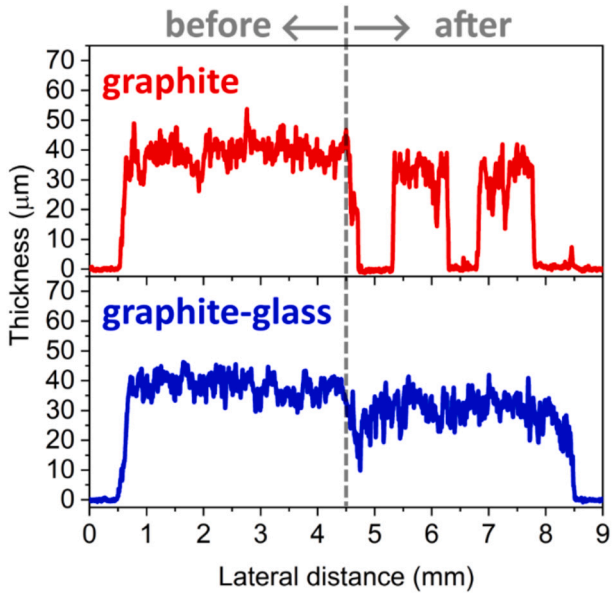

Fig. 2. The thickness of layer before (left) and after tape-test (right) for graphite and graphite-glass composite thick film on alumina.

Table 1
The average values and standard deviations of the graphite-glass thick-film thickness (t), surface roughness measured by profilometer (R_q) or by AFM (R_q^{AFM}) and sheet resistance (R_s) of WAP, WUVC and WTC.

Sample	WAP	WUVC	WTC
t [μm]	34 ± 0.9	34 ± 0.9	35 ± 0.9
R_q [μm]	3.1 ± 0.3	3.7 ± 0.3	3.3 ± 0.3
R_q^{AFM} [μm] 80 μm × 80 μm	2.0 ± 0.2	2.0 ± 0.5	2.3 ± 0.1
R_q^{AFM} [μm] 20 μm × 20 μm	1.0 ± 0.3	1.0 ± 0.2	0.8 ± 0.1
R_s [Ω/sq]	9.2 ± 0.3	9.0 ± 0.3	9.9 ± 0.4

The surface of the WAP, WUVC, and WTC was also examined using atomic force microscopy (AFM). This technique offers high-resolution images of the sample's surface, enabling direct measurement of surface topography and roughness, thereby delivering detailed insights into surface characteristics. A large scan size of 80 μm × 80 μm is selected to characterize the overall surface morphology, grain size and roughness of the sample, while a small scan size of 20 μm × 20 μm is selected to observe the morphology of the grains. The surface roughness determined by AFM, R_q^{AFM}, and summarized in Table 1, is an average value of R_q^{AFM} determined from AFM images taken at different locations, while in Fig. 4 and Fig. S1 the representative images of 20 μm × 20 μm and 80 μm × 80 μm scan size are shown, respectively.

The AFM images reveal that the surfaces of all WE are similar. The surface is homogeneous, showing the occurrence of irregularly shaped, randomly oriented grains with a size of a few to a few tens of μm, in agreement with particle size of the graphite and glass powders [11,12]. The light areas (LA) observed in the large-scale AFM images (Fig. S1a-c) are due to the AFM tip being unable to access certain regions because of the height variations, resulting in signal loss. This limited contact restricts the tip's ability to effectively probe the surface, which compromises measurement accuracy and can lead to incorrect topographical data. For instance, the R_q^{AFM} values determined from 80 μm × 80 μm regions were lower than the values obtained from contact profilometry. Moreover, the R_q^{AFM} values from 20 μm × 20 μm regions were even lower, as these measurements largely excluded areas with high roughness (Fig. 4, Fig. S1, Table 1). The similar morphology and surface

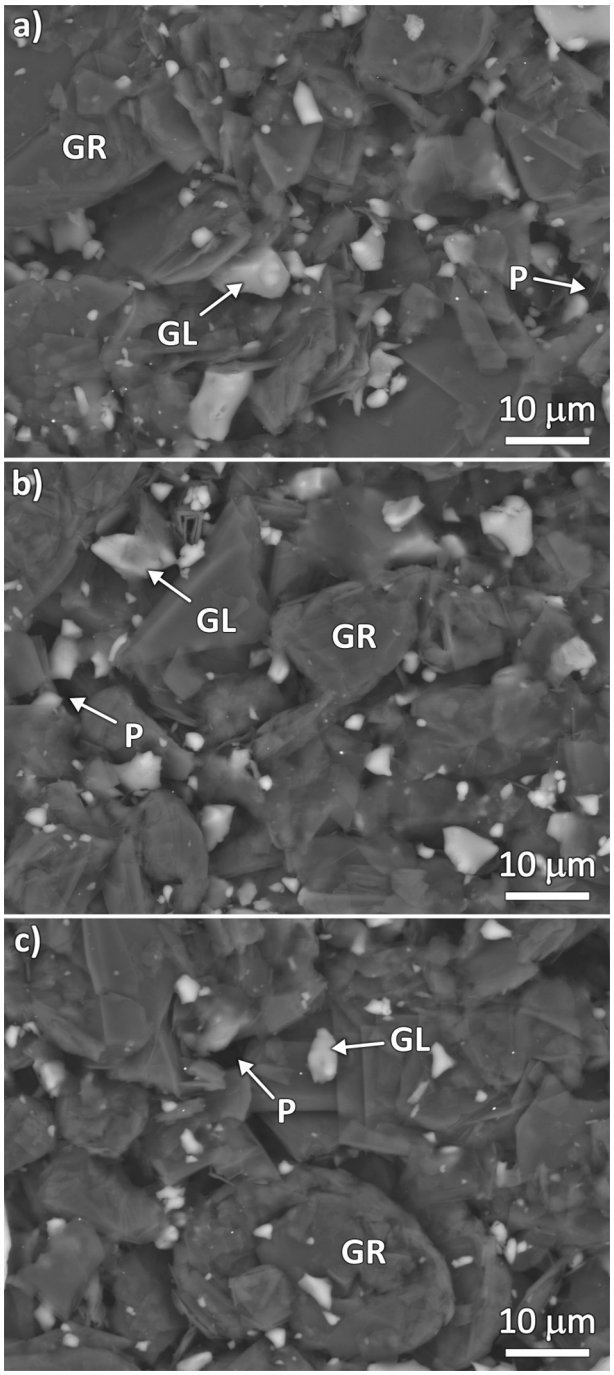

Fig. 3. a) SEM images of surfaces a) WAP, b) WUVC, and c) WTC. GR-graphite, GL-glass, P-pore.

roughness of WAP, WUVC, and WTC, as evaluated by both profilometry and AFM, suggest that there are no significant differences between them.

Prior to detail electrochemical analysis of the ES, we determine a working potential window (PW) of the AP, UVC and TC from the CVs measured in HCF (Fig. S2). Identical PW between −1.6 V and +1.0 V versus Pt quasi-reference electrode were determined for all three ESs (Fig. S3).

The cyclic voltammograms (CVs) measured in PBS and in HCF redox probe using ES with working electrodes WAP (AP), WUVC (UVC) and WTC (TC) are shown in Fig. 5 and the evaluated properties are summarized in Table 2.

It can be seen that all ESs show similar behaviour, with a good reversibility of the redox process with I_{pc}/I_{pa} close to unity. AP and UVC exhibit comparable I_{cap}, while TC exhibits smaller I_{cap}. Smaller I_{cap} could be related to the smallest electroactive surface area (A_{ecsa}) of TC, suggested also by smaller peak currents measured for these samples in HCF. AP and UVC exhibit similar ΔE_p values of ~115 mV, while ΔE_p of TC was larger, ~170 mV. The larger ΔE_p, along with the non-steep slope of the CV curve in the Faraday region, could indicate a reduced electron transfer rate (k^0) [12]. From characterization of CVs measured at different scan rates (ν) for AP, UVC, and TC, we obtained a linear relationship between I_p and $\nu^{1/2}$ (see Fig. S4) indicating that the redox process is controlled by the diffusion of the electroactive species to the WE surface in all cases. Since the peak potentials depend on the ν, and $n\Delta E_p$ ranged between 63 mV and 212 mV, the A_{ecsa} was calculated based on the modified Randles-Ševčík equation for quasi-reversible reaction [12,18,19]. The maximum values of A_{ecsa} and the corresponding A_{real} were obtained for the AP (Table 2). The A_{real} for UVC was comparable to AP, reaching approximately 95 % of the AP value. In contrast, the A_{real} for TC was substantially lower, 0.34 cm^2/cm^2_{geo}, accounting for only 27 % of the AP value. Interestingly, the A_{real} of AP and UVC was 1.5 times higher than that of commercially available ESs with graphite-based WEs [7], whose values range between 0.49 and 0.79 cm^2/cm^2_{geo}. The CVs measured at different ν were used to obtain a plot of ψ vs. $\nu^{-1/2}$ for the determination of k^0 [12,20]. Similar values for k^0 were obtained for AP and UVC, while the one for TC was lower and was only 23 % of AP value. The commercially available graphite-based electrodes [7] exhibit k^0 values that are lower, but in the same range as AP, UVC and TC, namely between 0.25 and 6.2 × 10^{-3} cm s^{-1}.

It is unlikely that the lowest electrochemical response of TC is due to surface morphology, as no significant differences in electrode morphology and roughness were found between the AP, UVC and TC samples (Fig. 4, Table 1). Thus, we investigated the chemical composition of the surface of the WAP, WUVC and WTC by the high-resolution XPS spectroscopy (HR-XPS). The spectra are shown in Fig. 6 and the atomic concentrations of the C and O are summarized in Table 3. The results reveal that the intensity of the C 1s peak at 284.4 eV and the O 1s peak at ~532 eV varied between the samples (Fig. 6a, b). WAP and WUVC contained similar amounts of C and O, while WTC contained less C and more O (Table 3). The highest O/C ratio for WTC indicates that the surface becomes oxygen-rich during heating at 150 °C in air. This suggests that lower electrochemical response of graphite-based WE after heating at 150 °C in air, as reflected in the larger ΔE_p, lower peak current, A_{ecsa} and k^0 (Fig. 5, Table 2), is related to the oxygen in the graphite layer.

To further investigate the influence of oxygen on the voltametric responses of AP, UVC and TC, CV scans were performed in the negative potential range where oxygen reduction is expected [23]. The initial measurements were performed with AP in PBS, saturated with either oxygen or nitrogen. In oxygen-saturated PBS, a clear peak at about −0.7 V was observed, while this peak was absent in nitrogen-saturated PBS (Fig. 7a) suggesting that it is attributed to the presence of oxygen in the solution. Fig. 7b and c show the CV of UVC and TC in nitrogen-saturated PBS. It is noteworthy that the current peak at −0.7 V is negligible. However, TC shows a current peak at about −0.8 V, whereas it is much less pronounced for AP or UVC. This current peak appears at a more negative potential compared to the one in oxygen-saturated solutions suggesting that it is associated with oxygen-containing groups at the carbon-based electrode surface. As well, the intensity of this current peak was the highest at TC, which is in agreement with the highest O/C ratio measured by XPS analysis (Table 3).

It is also interesting to mention that all ESs show the highest currents during the first cathodic scan, while the second and all subsequent scans have lower, but similar current response in PBS. Additionally, the peak current observed at −0.8 V during the first scan was absent in the following scans (see Fig. S5). This indicates that the amount of oxygen-containing groups within the carbon-based electrodes decreased after LSV to −1.5 V. The differences in response in PBS between the first and subsequent scans suggest that the electrode properties may change

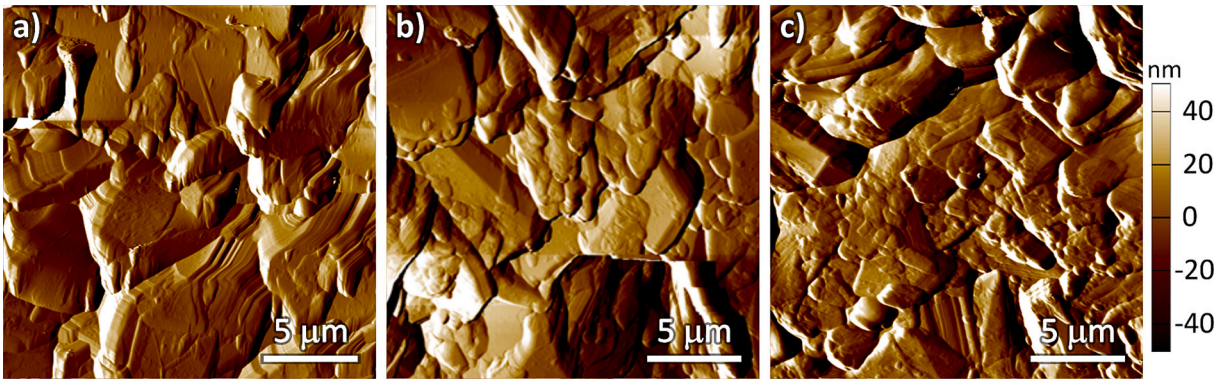

Fig. 4. AFM images of the a) WAP, b) WUVC, and c) WTC surface.

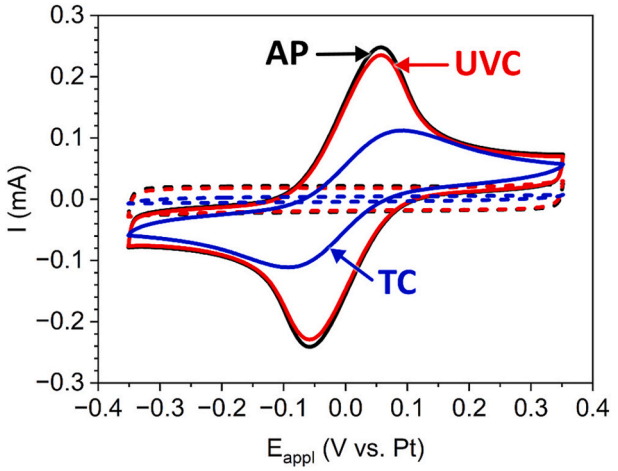

Fig. 5. Cyclic voltammograms of AP, TC, and UVC, recorded in PBS (blank, dashed lines) and HCF (solid lines) at 100 mV s^{-1} between −0.35 V and +0.35 V from initial potential −0.2 V in the positive direction.

Table 2
Summary of the electrochemical properties of the AP, UVC and TC obtained from the CVs recorded in HCF.

	AP	UVC	TC
I_{cap} [µA]	40.9 ± 1.3	37.7 ± 0.9	7.2 ± 0.9
I_{pc}/I_{pa}	1.14 ± 0.01	1.14 ± 0.00	1.06 ± 0.01
ΔE_p [mV]	115.6 ± 1.4	117.2 ± 2.4	169.3 ± 14.7
A_{ecsa} [cm^2]	0.63 ± 0.01	0.60 ± 0.01	0.22 ± 0.04
A_{real} [cm^2/cm^2_{geo}]	1.27	1.21	0.34
k^0 [10^{-3} cm s^{-1}]	7.92 ± 0.01	7.21 ± 0.09	1.78 ± 0.38

during the negative scan to −1.5 V. Therefore, we performed linear scan voltammetry (LSV) from 0.0 V to −1.5 V in HCF at 100 mV s^{-1} and subsequently investigated the voltametric response of AP, UVC and TC in a potential range between −0.35 and +0.35 V. The samples are denoted as AP-LSV, UVC-LSV and TC-LSV, respectively. AP-LSV and UVC-LSV exhibited similar response as AP and UVC, respectively. Interestingly, the response of TC-LSV was significantly improved compared to TC (Fig. S6, Fig. 5). Specifically, after the LSV the A_{ecsa} increased from 0.17 to 0.41 cm^2, and the k^0 rose from 2.12 to 5.32 × 10^{-3} cm s^{-1}. This could be attributed to lower amount of oxygen-containing groups in the electrode, but also to morphology changes upon LSV to −1.5 V. Thus, the surface of AP-LSV, UVC-LSV, and TC-LSV was analysed using AFM (Fig. 8 and Fig. S1d-e). The results indicate that the surface morphology of the electrodes after LSV differs from that prior to LSV. Specifically, the LSV appears to increase the surface roughness of

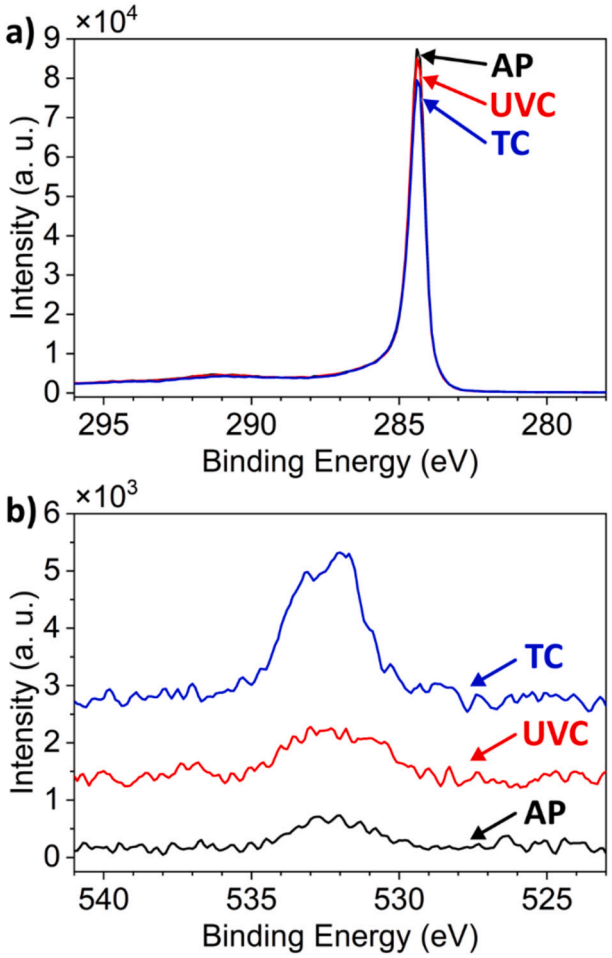

Fig. 6. HR-XPS spectra of a) C 1s and b) O 1s for WAP, WUVC and WTC.

Table 3
Surface composition and O/C ratio for WAP, WUVC and WTC.

	WAP	WUVC	WTC
C 1 s (at.%)	99.29 ± 0.01	99.40 ± 0.01	98.24 ± 0.17
O 1 s (at.%)	0.71 ± 0.01	0.60 ± 0.01	1.76 ± 0.17
O/C	0.007	0.006	0.018

all the samples, as summarized in Table S1. However, comparison of LSV treated samples show that the overall morphology and surface roughness of AP-LSV, UVC-LSV and TC-LSV were comparable with R_q^{AFM}

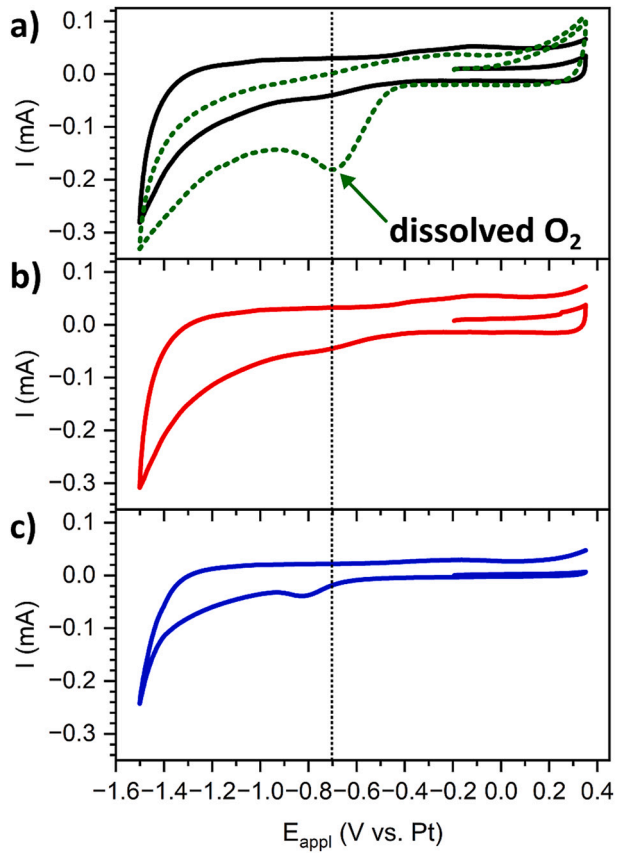

Fig. 7. Cyclic voltammograms (first scan) using AP (a), UVC (b), and TC (c), recorded in PBS saturated with nitrogen (solid lines) or oxygen (dashed line) at 100 mV s^{-1}.

values of 2.5 ± 0.6 μm and 1.3 ± 0.2 μm, measured over areas of 80 μm × 80 μm and 20 μm × 20 μm, respectively. Moreover, the comparable electrochemical responses observed for AP and AP-LSV, as well as UVC and UVC-LSV, indicate that surface roughness has negligible effect on the voltametric response (Fig. S6). Therefore, the improved performance of TC-LSV is likely predominantly due to differences in oxygen-containing group content rather than surface roughness effects.

The performance of the ESs was investigated in the solution of insecticide imidacloprid (IMD). The CVs measured in PBS and in IMD using AP, UVC and TC are shown in Fig. 9.

All CVs collected in IMD showed a cathodic peak I_{pc} at about −1.3 V, which can be ascribed to the irreversible reduction of the $-NO_2$ to −NHOH functional group [24]. An anodic peak I_{pa} at about −0.1 V observed in the second cycle, is related to the reoxidation of the reduced

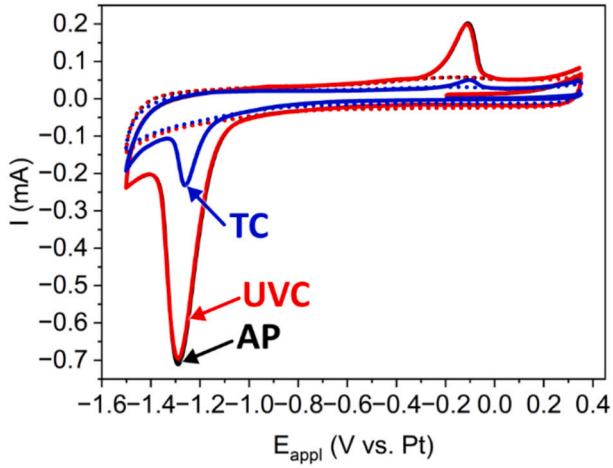

Fig. 9. Cyclic voltammograms of AP, UVC and TC, recorded in PBS (blank, dotted lines) and IMD (solid lines) at 100 mV s^{-1} between −1.5 V and +0.35 V from initial potential −0.2 V in the positive direction.

IMD [12]. The response of AP and UVC in IMD exhibited comparable I_{pc}, of −0.632 mV and − 0.616 mV, respectively. In comparison, the response of TC is reflected in a lower I_{pc} of −0.165 mV, which is only ~25 % of the I_{pc} of AP and UVC. The trends in the current response of AP, UVC and TC in IMD are similar to the trends in HCF, confirming that UV curing has minimal effect on the sensor performance, while heating to 150 °C in air significantly reduces it.

4. Conclusions

This study demonstrates that the post-deposition treating of electrochemical sensors with graphite-based working electrodes, which is necessary for the curing of the protective coating, significantly affects their electrochemical performance. The working electrodes, either as-prepared, or additionally UV or temperature cured, had comparable surface morphology and sheet resistance. The voltametric response of the investigated sensors showed that UV curing effectively preserved the electrochemical properties of the untreated sensor in the hexacyanoferrate redox probe, i.e., the peak current, the peak-to-peak potential separation ΔE_p, the electrochemically active surface area A_{ecsa} and the electron transfer rate constant k^0. In contrast, thermal treatment at 150 °C in air oxidises the graphite-based working electrode, which deteriorates the electrochemical properties of the sensor. Similar trends of reduced current response after heating the sensor to 150 °C in air were also observed for the insecticide imidacloprid, suggesting that UV curing has minimal effect on sensor performance, while temperature curing significantly reduces it. Electrochemical pretreatment with linear scan

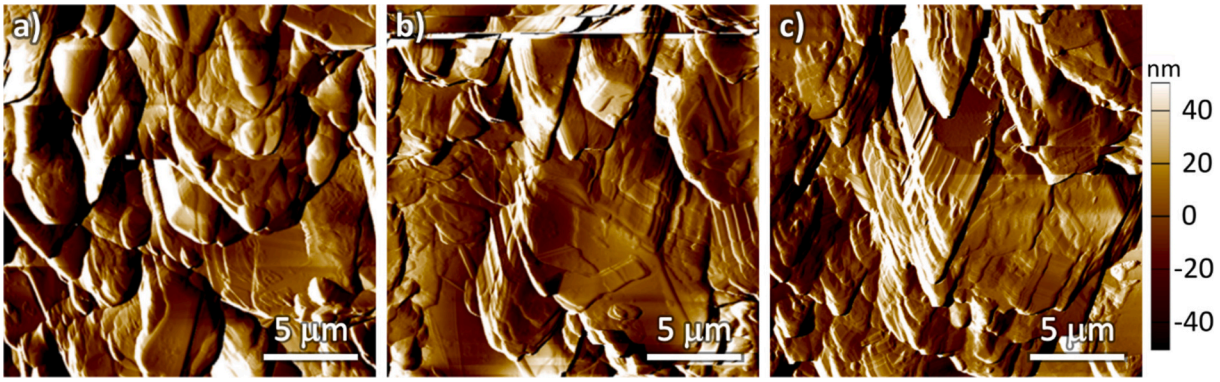

Fig. 8. AFM images of the a) WAP-LSV, b) WUVC-LSV and c) WTC-LSV surface.

voltammetry (LSV) to negative potentials of −1.5 V contributes to higher roughness of all working electrodes, but leads to similar electrochemical responses of the as-prepared and UV-cured sensors. However, LSV significantly improves the electrochemical response of the temperature-cured sensor, which is likely due to differences in the content of oxygen-containing groups in the working electrode rather than surface roughness effects. These results highlight the importance of optimising post-deposition curing protocols to advance the development of reliable, sensitive and selective electrochemical sensors for water pollution analysis.

CRediT authorship contribution statement

Danjela Kuscer: Writing – review & editing, Writing – original draft, Visualization, Validation, Supervision, Resources, Project administration, Methodology, Investigation, Funding acquisition, Conceptualization. **Barbara Repič:** Writing – review & editing, Writing – original draft, Visualization, Validation, Methodology, Investigation, Formal analysis. **Janez Kovač:** Resources, Investigation, Formal analysis. **Nejc Suban:** Investigation, Formal analysis. **Hana Uršič:** Writing – review & editing, Validation, Supervision, Resources.

Funding sources

This work was funded by the Slovenian Research and Innovation Agency through the research projects P2–0105, and Ministry of Higher Education, Science and Innovation of Republic Slovenia (C3360–23−252,004, M−ERA.NET).

Declaration of competing interest

The authors declare that they have no known competing financial interests or personal relationships that could have appeared to influence the work reported in this paper.

Acknowledgments

The authors thank dr. Layla Brini for screen printing and Val Fišinger for performing AFM analysis.

Appendix A. Supplementary data

Supplementary data to this article can be found online at https://doi.org/10.1016/j.inoche.2025.115669.

Data availability

Data will be made available on request.

References

[1] A.J. Bard, L.R. Faulkner, Electrochemical Methods: fundamentals and Applications, second ed., Wiley, New York, 2001.
[2] C.E. Banks, C.W. Foster, R.O. Kadara, Screen-Printing Electrochemical Architectures, Springer International Publishing, Cham, 2016, https://doi.org/10.1007/978-3-319-25193-6.
[3] R.D. Crapnell, C.E. Banks, Electroanalytical overview: screen-printed electrochemical sensing platforms, ChemElectroChem 11 (2024) e202400370, https://doi.org/10.1002/celc.202400370.
[4] V.A.R. Leite, S.P. de Oliveira, L.C. de Souza, L.J. de P. Silva, L.F. Silva, T.C. de O. Cândido, D.N. da Silva, A.C. Pereira, Development of novel conductive inks for screen-printed electrochemical sensors: enhancing rapid and sensitive drug detection, Analytica 6 (2025) 3, https://doi.org/10.3390/analytica6010003.
[5] A. García-Miranda Ferrari, S.J. Rowley-Neale, C.E. Banks, Screen-printed electrodes: transitioning the laboratory in-to-the field, Talanta Open 3 (2021) 100032, https://doi.org/10.1016/j.talo.2021.100032.
[6] R. Umapathi, S.M. Ghoreishian, S. Sonwal, G.M. Rani, Y.S. Huh, Portable electrochemical sensing methodologies for on-site detection of pesticide residues in fruits and vegetables, Coord. Chem. Rev. 453 (2022) 214305, https://doi.org/10.1016/j.ccr.2021.214305.
[7] R.O. Kadara, N. Jenkinson, C.E. Banks, Characterisation of commercially available electrochemical sensing platforms, Sensors Actuators B Chem. 138 (2009) 556–562, https://doi.org/10.1016/j.snb.2009.01.044.
[8] N.A. Choudry, D.K. Kampouris, R.O. Kadara, C.E. Banks, Disposable highly ordered pyrolytic graphite-like electrodes: tailoring the electrochemical reactivity of screen printed electrodes, Electrochem. Commun. 12 (2010) 6–9, https://doi.org/10.1016/j.elecom.2009.10.021.
[9] J.P. Metters, R.O. Kadara, C.E. Banks, Electroanalytical properties of screen printed graphite microband electrodes, Sensors Actuators B Chem. 169 (2012) 136–143, https://doi.org/10.1016/j.snb.2012.04.045.
[10] A. Mishra, Z. Ahmad, I. Zimmermann, D. Martineau, R.A. Shakoor, F. Touati, K. Riaz, S.A. Al-Muhtaseb, M.K. Nazeeruddin, Effect of annealing temperature on the performance of printable carbon electrodes for perovskite solar cells, Org. Electron. 65 (2019) 375–380, https://doi.org/10.1016/j.orgel.2018.11.046.
[11] B. Repič, K. Radan, G. Marolt, A.B. Golob, D. Kuscer, Effect of processing temperature on performance of screen-printed graphite electrodes, Mater. Chem. Phys. 337 (2025) 130455, https://doi.org/10.1016/j.matchemphys.2025.130455.
[12] B. Repič, G. Marolt, D. Kuscer, Carbon-based thick films for electrochemical detection of neonicotinoid insecticides, J. Electroanal. Chem. 984 (2025) 119054, https://doi.org/10.1016/j.jelechem.2025.119054.
[13] K. Grennan, A.J. Killard, M.R. Smyth, Physical characterizations of a screen-printed electrode for use in an amperometric biosensor system, Electroanalysis 13 (2001) 745–750, https://doi.org/10.1002/1521-4109(200105)13:8/9%253C745::AID-ELAN745%253E3.0.CO;2-B.
[14] R.R. Suresh, M. Lakshmanakumar, J.B.B. Arockia Jayalatha, K.S. Rajan, S. Sethuraman, U.M. Krishnan, J.B.B. Rayappan, Fabrication of screen-printed electrodes: opportunities and challenges, J. Mater. Sci. 56 (2021) 8951–9006, https://doi.org/10.1007/s10853-020-05499-1.
[15] F. Li, W. Xiong, C. Zhang, D. Wang, C. Zhou, W. Li, G. Zeng, B. Song, Z. Zeng, Neonicotinoid insecticides in non-target organisms: occurrence, exposure, toxicity, and human health risks, J. Environ. Manag. 383 (2025) 125432, https://doi.org/10.1016/j.jenvman.2025.125432.
[16] M. Dekleva, M. Kovačević, E. Gričar, M. Kolar, B. Genorio, B. Repič, D. Kuščer, H. Prosen, G. Marolt, An innovative pretreatment protocol to eliminate silver contamination-induced voltammetric interference on graphite-glass working electrode, Electrochem. Commun. 162 (2024) 107707, https://doi.org/10.1016/j.elecom.2024.107707.
[17] J.F. Moulder, J. Chastain (Eds.), Handbook of X-Ray Photoelectron Spectroscopy: a Reference Book of Standard Spectra for Identification and Interpretation of XPS Data, Update, Perkin-Elmer Corporation, Eden Prairie, Minn, 1992.
[18] H. Matsuda, Y. Ayabe, Zur Theorie der Randles-Sevčikschen Kathodenstrahl-Polarographie, Z. Für Elektrochem. 59 (1955) 494–503, https://doi.org/10.1002/bbpc.19550590605.
[19] M.G. Trachioti, A.Ch. Lazanas, M.I. Prodromidis, Shedding light on the calculation of electrode electroactive area and heterogeneous electron transfer rate constants at graphite screen-printed electrodes, Microchim. Acta 190 (2023) 251, https://doi.org/10.1007/s00604-023-05832-w.
[20] R.S. Nicholson, Theory and application of cyclic voltammetry for measurement of electrode reaction kinetics, Anal. Chem. 37 (1965) 1351–1355, https://doi.org/10.1021/ac60230a016.
[21] M. Zhiani, S. Kamali, Preparation and evaluation of nickel nanoparticles supported on the Polyvinylpyrrolidone-graphene composite as a durable Electrocatalyst for HER in alkaline media, Electrocatalysis 7 (2016), https://doi.org/10.1007/s12678-016-0330-1.
[22] M.-X. Qiao, Y. Zhang, L.-F. Zhai, M. Sun, Corrosion of graphite electrode in electrochemical advanced oxidation processes: degradation protocol and environmental implication, Chem. Eng. J. 344 (2018) 410–418, https://doi.org/10.1016/j.cej.2018.03.105.
[23] M. Gara, R.G. Compton, Activity of carbon electrodes towards oxygen reduction in acid: a comparative study, New J. Chem. 35 (2011) 2647–2652, https://doi.org/10.1039/C1NJ20612E.
[24] V. Guzsvany, F. Gaál, L. Bjelica, S. Ökrész, Voltammetric determination of imidacloprid and thiamethoxam, J. Serbian Chem. Soc. 70 (2005) 735–743, https://doi.org/10.2298/JSC0505735G.

Prof. dr. Danjela Kuščer, PhD in Materials Science, is a scientific councillor at the Jožef Stefan Institute and Professor at the Jožef Stefan International Postgraduate School, Slovenia. Her research focuses on the relationships between the processing and properties of ceramic, thick films by printing, solution-derived thin films and multilayer structures. She is author or co-author of about 150 scientific publications, 160 technical reports, 1 technical innovation and 7 patents. H-index: 25. She has actively participated in over 20 national and 15 international projects. She is the recipient of the national award for important applied research Puh recognition, national recognitions for innovation in ceramic materials and the Excellent in Science award.

Barbara Repič is currently a PhD student in the Electronic Ceramics Department at the Jožef Stefan Institute in Ljubljana. She obtained her BSc (2015) and MSc (2019) degrees in chemical engineering at the University of Ljubljana, where she specialized in materials science. Her research interests include processing of thick film structures, investigation of the relationship between processing and properties of ceramic, metal and carbon films, fabrication of electrochemical sensors, electrochemical characterization and sensor applications.

Prof. dr. Janez Kovač obtained a Ph.D. degree in Electronic Vacuum Technologies at the University of Maribor, Slovenia, in 2000. He is a Senior Research Associate at Jozef Stefan Institute and a lecturer at International Postgraduate School Jozef Stefan in Ljubljana, Slovenia. The main fields of scientific interest of Janez Kovac are reactions at solid surfaces, thin films and multilayer structures, plasma physics, high resolution XPS, SIMS and AES depth profiling, vacuum science, and technology. Janez Kovač is author and/or co-author of 350 publications in peer-reviewed international journals and has a H-index of 48.

Nejc Suban received his bachelor's and master's degrees in chemical engineering at the Faculty of Chemistry and Chemical Technology, University of Ljubljana, in 2022 and 2024, respectively, and is currently a PhD student at Jožef Stefan International Postgraduate School, Ljubljana, Slovenia. His research employs scanning probe microscopy techniques, including atomic force microscopy, piezoresponse force microscopy, and other advanced methods, to investigate piezoelectric and ferroelectric ceramic materials at the nanoscale.

Prof. dr. Hana Uršič Nemevšek is a tenured research associate at the Electronic Ceramics Department, Jožef Stefan Institute, and Associate Professor at the International Postgraduate School. She is the author of 130 scientific publications and 4 review papers. Her research topics focus on ceramic materials, including the aerosol deposition of thick films, lead-based and lead-free piezoelectric ceramics, and electrocaloric materials. She led 15 national and international projects, including bilateral cooperation. Her work has been cited ~3800 times with an h-index of 32 and an i10-index of 91.